Desalination and Water Treatment
www.deswater.com

doi: 10.1080/19443994.2015.1124055

57 (2016) 21564–21576
September

Taylor & Francis
Taylor & Francis Group

M-Al-SO_4 layered double hydroxides (M=Zn, Mg or Ni): synthesis, characterization and textile dyes removal efficiency

Fatima Zahra Mahjoubi[a,b], Abderrahim Khalidi[b], Mohamed Abdennouri[a], Noureddine Barka[a,*]

[a]*Laboratoire des Sciences des Matériaux, Univ Hassan 1, des Milieux et de la Modélisation (LS3M), BP 145, 25000 Khouribga, Morocco, Tel. +212 671 79 30 50; email: mahjoubi.fatimazahra@gmail.com (F.Z. Mahjoubi), Tel. +212 667 66 90 39; email: abdennourimohamed@yahoo.fr (M. Abdennouri), Tel. +212 661 66 66 22; Fax: +212 523 49 03 54; email: barkanoureddine@yahoo.fr (N. Barka)*

[b]*Laboratoire de Chimie Physique et de Chimie Bioorganique, Faculté des Sciences et Techniques, Université Hassan II de Casablanca, BP 146 Mohammedia, Morocco, Tel. +212 661 64 09 93; email: khalidiabderrahim1@gmail.com (A. Khalidi)*

Received 23 April 2015; Accepted 15 November 2015

ABSTRACT

Mg–Al, Zn–Al, and Ni–Al layered double hydroxides (LDH) materials with molar ratio (M^{2+}/Al^{3+}) of 3 were synthesized via co-precipitation method. The as-synthesized samples were characterized by X-ray diffraction (XRD), Fourier transform infrared spectroscopy (FTIR), transmission electron microscopy (TEM), and simultaneous thermogravimetric–differential thermal analysis (TGA/DTA). XRD analyses showed that Zn–Al-SO_4 had the greatest lattices parameters followed by Mg–Al-SO_4 and Ni–Al-SO_4. FTIR confirmed clearly the presence of sulfate anions in the structure of LDHs with the presence of carbonate impurity in the interlayer. TGA/DTA analysis indicates a better thermal stability of Zn–Al-SO_4 vs. Ni–Al-SO_4 and Mg–Al-SO_4. The capability of the materials for textile dye removal was investigated using methyl orange (MO) as a model dye and an industrial textile effluent. Experimental results showed that pH is the most affecting factor in dye removal. The effective pH range for dye removal was between 3.5 and 5. The adsorption process can be well described by the pseudo-second-order kinetic model. The Langmuir model fit equilibrium data with exceptional maximum adsorption capacities for MO of 2,758, 1,622, and 800 mg/g, respectively, in the case of Zn–Al-SO_4, Mg–Al-SO_4, and Ni–Al-SO_4. Color and chemical oxygen demand (COD) reduction from industrial textile effluent increased with the increase in the amount of LDHs. The optimum color and COD reduction were obtained by Zn–Al-SO_4.

Keywords: Layered double hydroxides; Synthesis; Characterization; Adsorption; Textile effluent

1. Introduction

Discharging large quantities of dyes in water resources from various dyestuff manufactures, plastic, and paper-making industries pose serious environmental problems. Because of its complex characteristics, such as a high concentration of organic pollutants, deep chromaticity, low biodegradability and complex ingredients, dyeing wastewater is difficult to treat by conventional wastewater treatment processes [1]. Several methods have been investigated for textile

*Corresponding author.

wastewater (TWW) treatment, including biological treatment [2], coagulation/flocculation [3], chemical oxidation [4], membrane filtration [5], ion exchange [6], photocatalytic degradation [7], and adsorption [8]. Of these techniques, adsorption is a common method for dye removal because it is effective and economical [9]. So far, common adsorbents, such as natural biomaterials [10], activated carbon [11], natural phosphate [12], clay [8], and polymers [13], have been investigated and found to be capable of removing dyes from wastewater. In terms of initial cost, simplicity of design, ease of operation, and insensitivity to toxic substances, clay derivatives have been considered as one of the most appropriate sorbents [14,15].

In recent decades, a class of anionic clays known as layered double hydroxides (LDHs) or hydrotalcite-like compounds has attracted considerable attention. The general formula for an LDH is $[M^{II}_{(1-x)}M^{III}_{x}(OH)_2]\cdot[A^{n-}_{x/n}\cdot mH_2O]$, where M^{II} represents a divalent metal such as Mg, Ni, Mn, Fe, Co, Cu, and Zn, M^{III} represents a trivalent metal such as Al, Fe, Cr, Mn, and Co, and x equal to the $M^{III}/(M^{II}+M^{III})$ molar fraction generally ranging from 0.17 to 0.33. An enormous variety of interlayer anions (A^{n-}) can be incorporated in LDHs [16]. They range from simple inorganic anions, such as PO_4^{3-}, CO_3^{2-}, SO_4^{2-}, NO_3^-, F^- or Cl^-, and organic anions such as dodecylsulfate and terephthalate [17–20]. From a structural viewpoint, the effect of divalent/trivalent cations and interlayer anionic composition may provide insights regarding the crystal chemistry of different LDH types, which may ultimately govern their ability to adsorb organic pollutant. From the above-cited inorganic anions, sulfate-based LDHs are significantly expandable, partly because of a high capacity to gain and lose water molecules [21,22]. This property favors anionic exchange processes and accounts for the environmental effectiveness in natural systems.

In the present work, Mg–Al, Zn–Al, and Ni–Al LDHs with SO_4^{2-} in the interlayer were synthesized by co-precipitation method. The synthesized samples were evaluated for the removal of methyl orange (MO) from aqueous solution. The effect of solution pH, contact time, and initial dye concentration were investigated in batch mode. Kinetic and equilibrium parameters were determined to understand the adsorption mechanism. To verify the efficacy of the materials for TWW treatment, adsorption experiments were conducted with industrial dye wastewater from a printing and dyeing factory. The effects of various parameters on the removal of color and chemical oxygen demand (COD) such as solution pH and adsorbent dose were studied in detail.

2. Materials and methods

2.1. Materials

All the chemicals used were of analytical grade. $Zn(NO_3)_2{\cdot}6H_2O$ (>98% purity), $Ni(NO_3)_2{\cdot}6H_2O$, $Mg(NO_3)_2{\cdot}6H_2O$, $Al(NO_3)_3{\cdot}9H_2O$ (>98% purity), Na_2SO_4, NaCl, and MO were purchased from Sigma-Aldrich (Germany). NaOH was purchased from Merck (Germany), and HNO_3 from Scharlau (Spain). Solutions were prepared using deionized water.

2.2. Preparation of layered double hydroxides

The sulfates containing LDHs with molar ratio M^{2+}/Al^{3+} of 3 were prepared by the co-precipitation method. A solution containing 100 ml of Zn $(NO_3)_2{\cdot}6H_2O$, $Ni(NO_3)_2{\cdot}6H_2O$ or $Mg(NO_3)_2{\cdot}6H_2O$ (0.75 M) and $Al(NO_3)_3{\cdot}9H_2O$ (0.25 M) was added drop wise to a solution containing 100 ml of NaOH (2 M) and (0.2 M) of Na_2SO_4 under vigorous stirring at pH 10.0 for 2 h. The resultant slurries were treated hydrothermally at 80°C for 24 h, washed repeatedly with decarbonated water, and dried at 60°C for 12 h. The obtained materials were powdered and referred as Zn–Al-SO_4, Mg–Al-SO_4, and Ni–Al-SO_4.

2.3. Characterization

Powder X-ray diffraction (XRD) patterns were recorded from $2\theta = 5$ to 70° using a Bruker-axs D2-phaser advance diffractometer operating at 30 kV and 10 mA with Cu Kα1 (1.54056 Å) and Kα2 (1.54439 Å) radiations. Fourier transform infrared spectroscopy (FTIR) spectra were collected on a Nicolet Avatar 330 Fourier transform IR spectrophotometer. Samples were mixed with KBr for a mass ratio of 1:100 and finely powdered to prepare pellets. The spectra were recorded with 2 cm^{-1} resolution in the range of 4,000–400 cm^{-1}. Transmission electron microscopy (TEM) images were obtained on a TEM TECNAI G2/FEI instrument, at accelerating voltage of 120 kV. Simultaneous thermogravimetric–differential thermal analysis (TGA-DTA) curves were recorded on a SETARAM (SENSYSevo) instrument under argon atmosphere in the temperature range of 30–700°C at a heating rate of 10°C/min. The point of zero charge (pH_{PZC}) was determined by the pH drift method according to the method proposed by Noh and Schwarz [23]. The pH of NaCl aqueous solution (50 mL at 0.01 mol/L) was adjusted to successive initial values from 2.0 to 12.0 by the addition of HNO_3 (0.1 N) and/or NaOH (0.1 N). More there, 0.05 g of each LDH was added in 50 mL of solution and stirred for 6 h. The final pH

was measured and plotted against the initial pH. The pH_{PZC} was determined at the value for which $pH_{final} = pH_{initial}$.

2.4. Adsorption tests

2.4.1. Study of MO removal

Stock solutions of 1 g/L of MO were prepared by dissolving appropriate amount of the dye in distilled water and the used concentrations were obtained by dilution. Adsorption experiments were performed in a series of 500 mL beakers containing the desired weight (20 mg) of each LDHs and 250 mL of the MO solution at the desired concentration. These experiments were carried out at a constant agitation speed of 500 rpm by varying the pH of solution from 2 to 12. The contact time was varied from 5 to 360 min and the initial dye concentration from 20 to 1,000 mg/L. The solution pH was adjusted to a given value by the addition of HNO_3 (1 N) or NaOH (1 N) and was measured using a SensION+ PH31 pH meter.

After each adsorption experiment was completed, the solid phase was separated from the liquid phase by centrifugation at 3,000 rpm for 15 min. The residual concentrations of MO were determined from UV–vis characteristics at maximum absorption wavelength $\lambda_{max} = 465$ nm using a TOMOS V-1100 UV–vis spectrophotometer.

The adsorbed amounts of MO were calculated using the following equation:

$$q = (C_0 - C)V/m \quad (1)$$

where q (mg/g) is the adsorbed quantity, C_0 (mg/L) is the initial dye concentration, C (mg/L) is the dye concentration at a time t, and V (L) the volume of solution and m (g) is the mass of adsorbent.

2.4.2. Treatment of wastewater samples

TWW sample at the factory's discharge point was collected from a cotton and polyester textile mill ITEX, Casablanca, Morocco. The sample was stored at temperature ≤5°C to avoid any change in its physicochemical characteristics before use. Treatment experiments were performed in a series of 50 mL beakers containing the desired dose of LDHs ranging between 0.5 and 5.0 g/l and 20 mL of wastewater. The experiments were carried out at constant agitation speed of 500 rpm for 8 h. The pH was evaluated in the same conditions used in the adsorption MO experiments.

Dye removal from TWW was estimated from the change in UV–vis absorbance in the range of 200–700 nm using a BIOCHROM BIBRA Light spectrophotometer. The COD of supernatant was analyzed by potassium dichromate oxidation method [24]. The percentage of COD removal (%COD) was calculated by the following equation:

$$\%COD = \frac{COD_0 - COD}{COD_0} \times 100 \quad (2)$$

where COD_0 and COD both in (mg/L) are the COD before and after treatment.

3. Results and discussion

3.1. Characterization

3.1.1. XRD analysis

XRD patterns of the samples, shown in Fig. 1, exhibit characteristic reflections of clay minerals possessing a layered structure similar to the pattern of natural hydrotalcite layered double hydroxides. The diffraction peaks were indexed to a hexagonal lattice with rhombohedral 3R symmetry [16]. The sharpness of (0 0 l) peaks becomes weaker in Mg–Al-SO_4 and Ni–Al-SO_4 which should be related to the reduction in crystallinity of these samples. The high peaks at low 2θ values, indicating characteristic basal reflections of SO_4^{2-} LDH materials, were also observed. The XRD pattern also showed $Zn(OH)_2$ and $Al(OH)_3$ crystalline impurities in samples, which can be identified by comparison of their characteristic diffraction pattern to a reference library of patterns. These impurities in the sample may result from poor control of the pH during the synthesis because ZnAl LDHs are generally obtained at pH lower than 10.

The lattice parameters a and c are calculated from the diffraction plane positions of $d(0\,0\,3)$ and $d(1\,1\,0)$ as follows: $c = 3d(0\,0\,3)$ and $a = 2d(1\,1\,0)$. The obtained parameters are summarized in Table 1. A comparison of the Zn–Al-SO_4, Mg–Al-SO_4, and Ni–Al-SO_4 systems demonstrates a considerable difference in parameter "a" of the samples, and the lattice parameter "a" of the Zn–Al-SO_4 was 3.05 Å greater than Mg–Al-SO_4 (3.04 Å) and the Ni–Al-SO_4 (3.03 Å). These observed differences in "a" parameters are in agreement with Vegard's law for solid solutions, which corroborates the inclusion of metal cations into the LDH sheet. The ionic radius of Zn^{2+} (0.74 Å) was greater than ionic radius of Mg^{2+} (0.72 Å) and Ni^{2+} (0.69 Å) [25].

Similar to findings for the "a" parameter, the "c" parameter was greater in the Zn–Al-SO_4 (33.47 Å) than

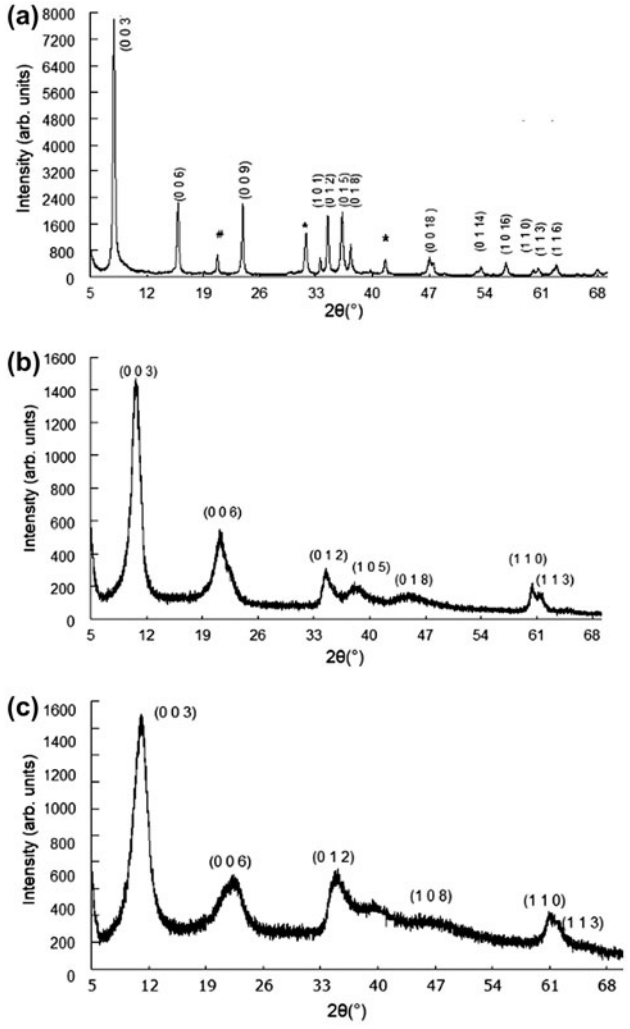

Fig. 1. XRD patterns of the LDH samples: (a) Zn–Al-SO_4, (b) Mg–Al-SO_4, (c) Ni–Al-SO_4, (*) $Zn(OH)_2$, and (#) Al $(OH)_3$.

Table 1
Calculated unit cell parameters of the LDHs

Sample	Unit cell parameters (Å)		Interlayer distance (Å)
	c	*a*	*d*
Zn–Al-SO_4	33.47	3.05	11.15
Mg–Al-SO_4	24.96	3.04	8.32
Ni–Al-SO_4	24.05	3.03	8.01

the Mg–Al-SO_4 (24.96 Å) and Ni–Al-SO_4 (24.05 Å). At this point, it is important to note that c distance depends on the size and intercalation degree of interlayer anions, and on the layer charge density to a lesser degree. Furthermore, the greater interlayer distance in Zn–Al LDHs may indicate the formation of an anionic bilayer. Since the value of *c* is less, interlayer thickness in the Ni system is less. Because the synthesis was carried out in atmospheric condition, some CO_3^{2-} was incorporated into the LDHs (see discussion below).

3.1.2. Transmission electron microscopy

Fig. 2 presents TEM images of different LDH samples. As demonstrated in the figure, the Zn–Al-SO_4 sample exhibited mainly perfect hexagonal platelet structures, having some small cracks at the edge of hexagonal sheets and part of sheets presenting vertical crossing at hexagonal sides. The particle size varied from 20 to 150 nm. TEM micrographs for Ni–Al-SO_4 and Mg–Al-SO_4 indicate the formation of agglomerate structure formed by the smallest particles, which was detected at reduction in the crystallinity phases by XRD.

3.1.3. TGA–DTA analysis

The thermal behavior of the three LDHs was examined using thermogravimetric analysis and differential thermal analysis. The results are illustrated in Fig. 3, and the weight loss percentages are calculated and summarized in Table 2. Four major decomposition stages can be considered; the first stage occurred at temperature ≤150˚C constituting of 6.02, 6.01, and 5.80% loss for Zn–Al-SO_4, Ni–Al-SO_4, and Mg–Al-SO_4, respectively. These mass losses are attributed to the removal of physisorbed water on the external surface of the layered double hydroxide. The second stage occurred between 150 and 250˚C constituting of 5.63, 8.61, and 4.94% loss for Zn–Al-SO_4, Ni–Al-SO_4, and Mg–Al-SO_4 respectively, which is due to loss of strongly held interlayer water molecule. The third stage of weight loss around 350˚C constituting of 2.00, 6.80, and 3.22% can be attributed to the removal of the carbonate incorporated in the structure of Zn–Al-SO_4, Ni–Al-SO_4, and Mg–Al-SO_4, respectively. The presence of this anion with high amount in Ni–Al-SO_4 and Mg–Al-SO_4 reduces the interlayer distance, which was confirmed by XRD analysis. The final stage of weight losses of 10.69, 12.33, and 15.07 at 500, 540, and 520˚C, respectively, for Zn–Al-SO_4, Mg–Al-SO_4, and Ni–Al-SO_4 is related to the brucite-like sheet decomposition and interlayer SO_4^{2-} loss. The greatest amounts of the sulfate present in Ni–Al-SO_4 (15.07%) and Mg–Al-SO_4 (12.33%) are partly responsible for the low crystallinity observed in XRD and the presence of the agglomerate structure observed in TEM micrographs.

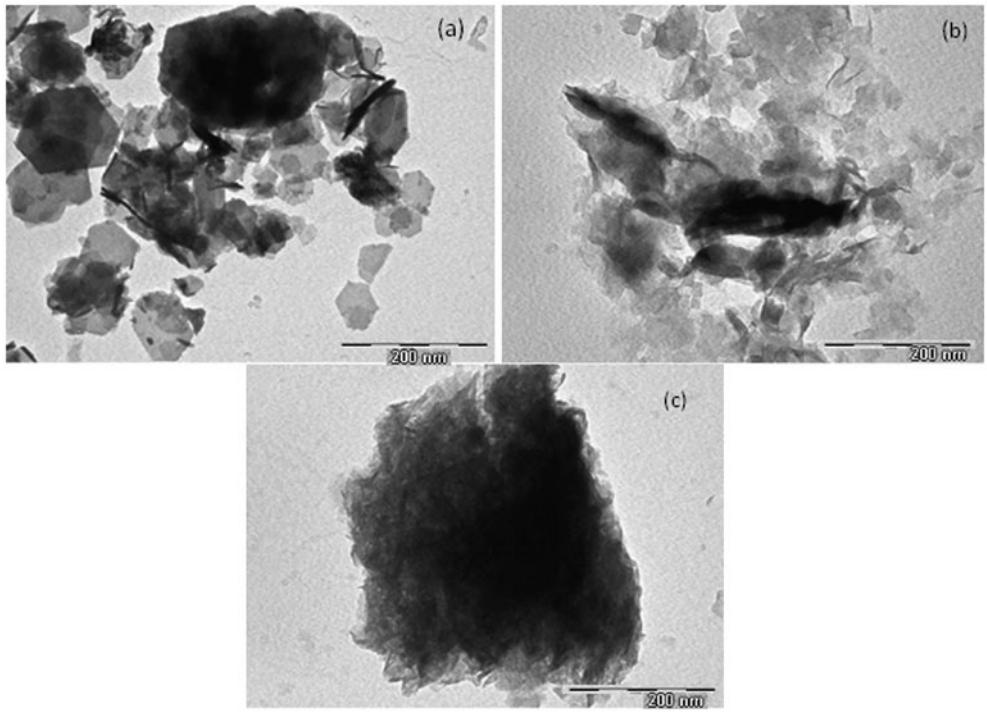

Fig. 2. TEM micrographs of the LDHs samples: (a) Zn–Al-SO_4, (b) Mg–Al-SO_4, and (c) Ni–Al-SO_4.

The differences existing among the thermal stability patterns with a total mass loss at 700˚C was 26.60, 33.70, and 29.10% for Zn–Al-SO_4, Mg–Al-SO_4, and Ni–Al-SO_4, respectively. This suggests comparatively less mass loss occurred in case of Zn containing layered double hydroxide compared to the Ni and Mg containing LDHs. This result is commonly observed by Sanchez Valente et al. for the thermal decomposition of hydrotalcites containing different metallic compositions [26]. It was found that the temperature of interlayer anion decomposition of Mg–Al-SO_4 (530˚C) and Ni–Al-SO_4 (520˚C) is greater than Zn–Al-SO_4 (500˚C), suggesting the binding force between basic layer and the interlayer space of Mg–Al-SO_4 and Ni–Al-SO_4 compared with Zn–Al-SO_4.

3.1.4. FTIR

IR spectra have been used successfully to understand the distribution of anions in the interlayer and nature of bending vibration [27,28]. The FTIR spectrums for LDH samples are shown in Fig. 4. The figure reveals characteristic bands of hydrotalcite-like compounds. For all the samples, the H-O stretching vibration was observed around 3,500–3,550 cm^{-1}, which indicates that the OH^- groups present in the interlayer water molecules are not free but are held by H-bonding [16]. The band observed at 1,670 cm^{-1} is due to an H_2O-deformation in interlayer structure [29] and is slightly shifted to greater wave numbers in the case of Mg^{2+} vs. Ni and Zn^{2+} containing LDHs. These results align with the high amount of H_2O in interlayer structure confirmed by TGA–DTA analysis. The IR spectra of the LDHs show the presence of active $v_3(CO_3^{2-})$ asymmetric stretch bands of carbonate, at ≈1,390, 1,409, and 1,410 cm^{-1} for Zn–Al-SO_4, Mg–Al-SO_4, and Ni–Al-SO_4, respectively [30]. The presence of this band suggests the incorporation of CO_3^{2-} from the atmosphere. The intensity of this band is markedly important in the Ni–Al-SO_4 comparable to the two other samples, which may be responsible for the decrease in the lattice parameter "*c*". A comparison of the IR spectral bands of the SO_4^{2-}-containing LDHs shows distinct differences between 600 and 1,200 cm^{-1}. The $v_3(SO_4^{2-})$ vibration band (±1,100 cm^{-1}) is strongly active in Mg–Al-SO_4 and Zn–Al-SO_4, but the low intensity of this band in Ni–Al-SO_4-type LDHs indicates a different nature of the interlayer SO_4^{2-} [27]. The $v_1(SO_4^{2-})$ vibration band around 1,000 cm^{-1} represents a weak symmetric stretching. The vibrational bands around 700 and 900 cm^{-1} in the samples are assigned to Al-OH bending vibrations [31–34].

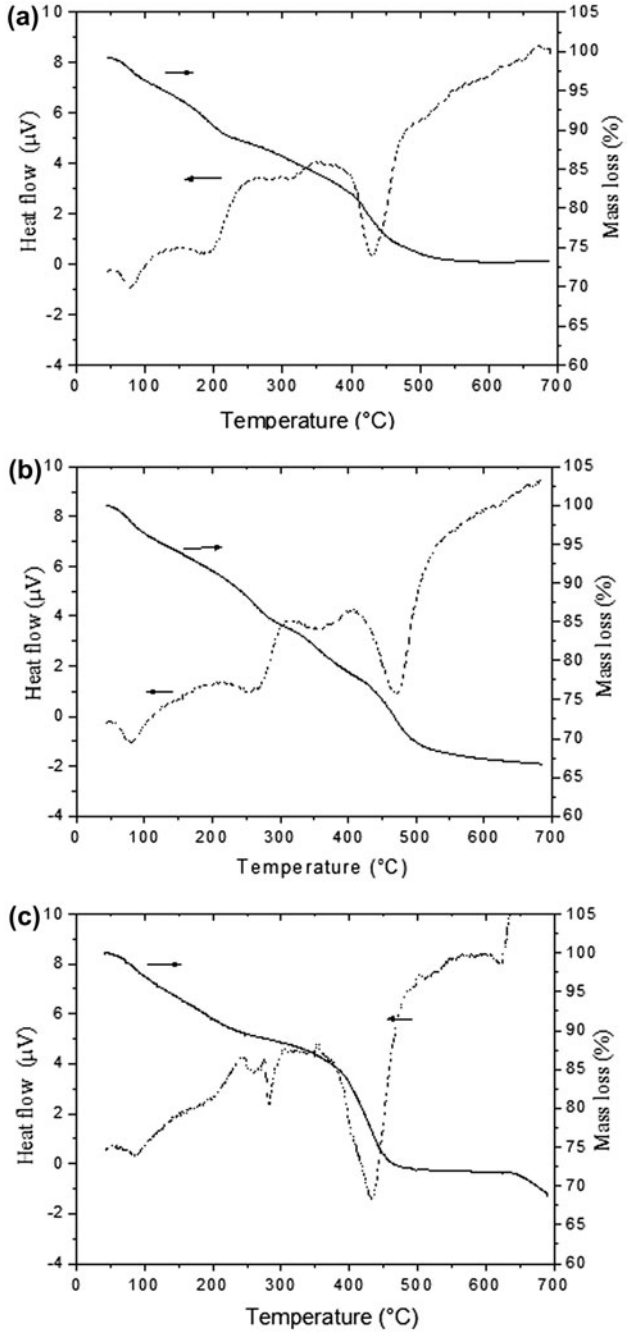

Fig. 3. TGA–DTA analysis of Zn–Al-SO_4 (a), Mg–Al-SO_4 (b), and Ni–Al-SO_4 (c).

3.2. Study of MO removal from aqueous solution

3.2.1. Effect of the solution pH

Fig. 5 shows the effect of pH on adsorption of MO onto Zn–Al-SO_4, Mg–Al-SO_4, and Ni–Al-SO_4. The optimum pH values for Zn–Al-SO_4, Mg–Al-SO_4, and Ni–Al-SO_4 were found to be 4.5, 4.7, and 3.5, respectively. Between pH 4 and 10, the adsorption amount decreased with increasing solution pH. The effect of pH solution on dye adsorption can be explained in terms of the point of zero charge (PZC) and the pKa of MO. The PZC is the pH where the net total particle charge is zero and can be used as a qualitative parameter for the adsorbent surface charge balance. The PZC of LDHs was 7.6, 7.5, and 7.4 for Zn–Al-SO_4, Mg–Al-SO_4, and Ni–Al-SO_4, respectively. Along with the positive charge that results from the structure of LDHs, the samples have variable charges that result from the adsorption of ions from the solution, such as H^+ or OH^-. For pH values below the PZC, hydrated surface of the LDHs is protonated and is positively charged. The surface of LDHs is deprotonated at pH values above the PZC and is negatively charged.

Furthermore, in the aqueous solution, the dissociation constant pK_a for MO is 3.46, and MO molecules were predominantly present as monovalent anions above this value of pH. At pH values below the PZC of LDHs and above pK_a of MO, there may be two possible processes for dye adsorption onto LDHs: one of them is anionic exchange of SO_4^{2-} anions in the interlayer by dye anions and the other is adsorption by means of association between the positively charged surface of LDH and the dye anions. For pH values above the PZC, the deprotonation of the surface hydroxyl groups and the charge positive on the surface of LDH decrease and the removal of the dye also decreases. Furthermore, the anionic dye must be in competition with the OH^- in the solution for exchange with the SO_4^{2-} anions that are associated with the surface. Because Mg, Zn, Ni, and Al dissolves at low pH medium, the LDHs structure can be destroyed; in this case, adsorption of MO on LDHs decreases.

3.2.2. Effect of contact time

The adsorption kinetics is important for the adsorption studies because it can describe the rate removal of adsorbate by LDHs and controls the equilibrium time. The kinetics of adsorption of MO onto LDHs samples is shown in Fig. 6. The results reveal that the adsorption is fast in the initial 60 min, and it gradually becomes slower with contact time until reaching equilibrium. The affinity of dye ions toward Mg–Al-SO_4 is more important than that of Zn–Al-SO4 and Ni–Al-SO_4. The rapid adsorption at the initial contact time is due to the existence of a number of vacant sites on the surface that are available for adsorption during the initial stage. The later slow rate of MO adsorption is probably due to the anionic exchange between the methyl and interlayer sulfate anion.

Table 2
Weight loss percentages for Zn–Al-SO_4, Mg–Al-SO_4, and Ni–Al-SO_4

Samples	First weight loss (%)			Second weight loss (%)			Third weight loss (%)			Last weight loss (%)			Total weight loss (%)
	Onset (°C)	Offset (°C)	Wt loss (%)	Onset (°C)	Offset (°C)	Wt loss (%)	Onset (°C)	Offset (°C)	Wt loss (%)	Onset (°C)	Offset (°C)	Wt loss (%)	
Zn–Al-SO_4	50	150	6.02	150	250	5.63	250	350	2.00	350	500	10.69	26.60
Mg–Al-SO_4	50	150	6.01	150	270	8.61	270	400	6.80	400	540	12.33	33.70
Ni–Al-SO_4	50	150	5.80	150	250	4.94	250	350	3.22	350	520	15.07	29.10

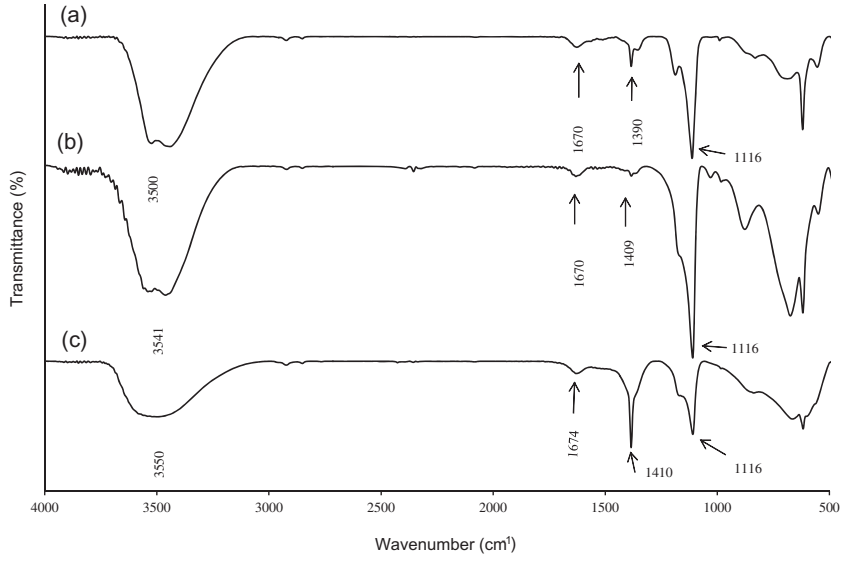

Fig. 4. FTIR spectra Zn–Al-SO_4 (a), Mg–Al-SO_4 (b), and Ni–Al-SO_4 (c).

In order to characterize the kinetics involved in the process of adsorption, pseudo-first-order, pseudo-second-order, and intraparticle diffusion models rate equations were proposed and the kinetic data were analyzed based on the regression coefficient (r^2) and the amount of dye adsorbed per unit weight of the adsorbent.

The first-order rate expression of Lagergren based on solid capacity is generally expressed as follows [35]:

$$q = q_e(1 - e^{-K_1 t}) \tag{3}$$

where q_e and q (both in mg/g) are, respectively, the amounts of dye adsorbed at equilibrium and at any time "t", and K_1 (1/min) is the rate constant of adsorption.

The pseudo-second-order model proposed by Ho and McKay [36] was used to explain the adsorption kinetics. This model is based on the assumption that the adsorption follows second-order chemisorption. The pseudo-second-order model can be expressed as:

$$q = \frac{K_2 q_e^2 t}{1 + K_2 q_e t} \tag{4}$$

where K_2 (g/mg min) is the rate constant of pseudo-second-order adsorption.

The experimental parameters and correlation coefficient R^2 are listed in Table 3. As can be seen from the table, the two models give a reasonably good fit to the experimental data, but comparison of the R^2 values indicates that the pseudo-second-order model gives the best overall fit. Furthermore, the calculated values of q_e using this model are also in good agreement with the experimental values. The best fit for the experimental data for all studied concentration values

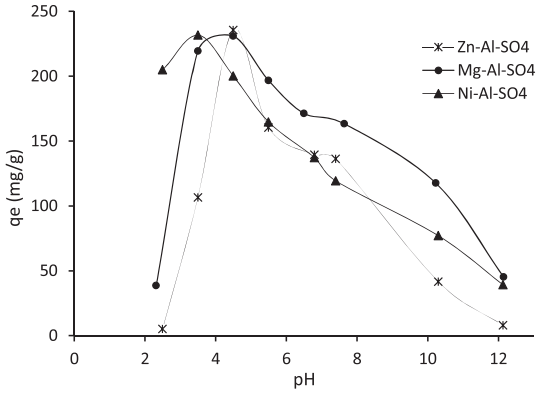

Fig. 5. Effect of solution pH on MO removal by Zn–Al-SO_4 (a), Mg–Al-SO_4 (b), and Ni–Al-SO_4 (c) (adsorbent dose: 80 mg/L, contact time: 8 h, initial MO concentration: 20 mg/L, temperature: 25°C, and agitation speed: 500 rpm).

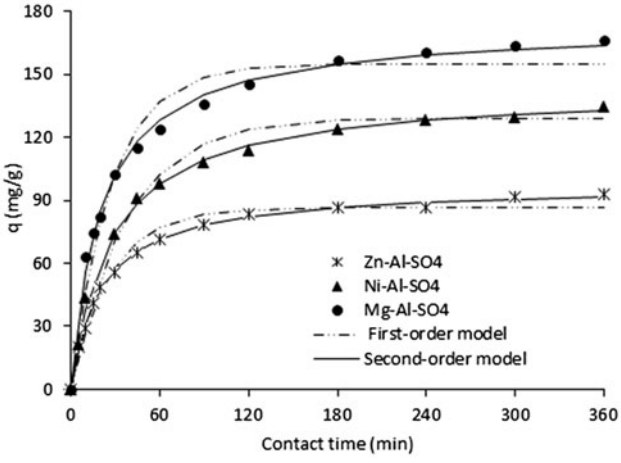

Fig. 6. Kinetics of MO adsorption onto LDH samples (adsorbent dose: 80 mg/L, initial MO concentration: 20 mg/L, solution pH 8, temperature: 25°C, and agitation speed: 500 rpm).

confirms that the velocity control mechanism of adsorption is chemical adsorption. Similar results for other types of dyes and other contaminants adsorbed in LDHs are found in the literature [37].

To identify the diffusion mechanism in the adsorption of MO ions on LDHs, intraparticle mass transfer diffusion model proposed by Weber and Morris [38] was used. This model is expressed by the following equation:

$$q = k_i t^{1/2} + C \quad (5)$$

where k_i (mg/g $\text{min}^{0.5}$) is the rate constant and obtained from the slope of the straight line of q vs. $t^{0.5}$. C is the intercept which gives an idea about the thickness of boundary layer, the larger the intercept, the greater the boundary layer effect.

Fig. 7 shows the intraparticle diffusion model for the adsorption of MO onto LDH samples. The plots are not linear over the complete time range, suggesting that more than one process affects the adsorption. Such type of plots presents multilinearity, indicating that three steps take place. The first is the instantaneous adsorption or external surface adsorption stage, which was controlled by initial MO concentration difference. The second region is the gradual adsorption stage where intraparticle diffusion is the rate-limiting step. The third stage is the final equilibrium where intraparticle diffusion further slows down due to the extremely low adsorbate concentrations left in the solutions.

3.2.3. Adsorption isotherms

The equilibrium adsorption capacities for MO increased with a rise in initial dye concentration, as shown in Fig. 8. The increase in adsorption amounts with concentration is probably due to a high driving force for mass transfer. In fact, high concentration in solution implicates large amounts of dye molecules fixed at the surface of the adsorbent. The isotherm form was type L in Giles classification [39]. These types of isotherms are usually associated with ionic

Table 3
Pseudo-first-order model and pseudo-second-order model parameters for MO adsorption by LDHs

		Pseudo-first-order model			Pseudo-second-order model		
Adsorbent	$q_{e,exp}$ (mg/g)	$q_{e,cal}$ (mg/g)	K_1 (1/min)	R^2	$q_{e,cal}$ (mg/g)	K_2 (g/mg min)	R^2
Zn–Al-SO_4	92.72	86.65	0.03641	0.9798	97.003	0.00049	0.9979
Mg–Al-SO_4	166.39	154.73	0.03605	0.9617	172.857	0.00028	0.9952
Ni–Al-SO_4	134.65	129.15	0.02629	0.9778	144.427	0.00023	0.9934

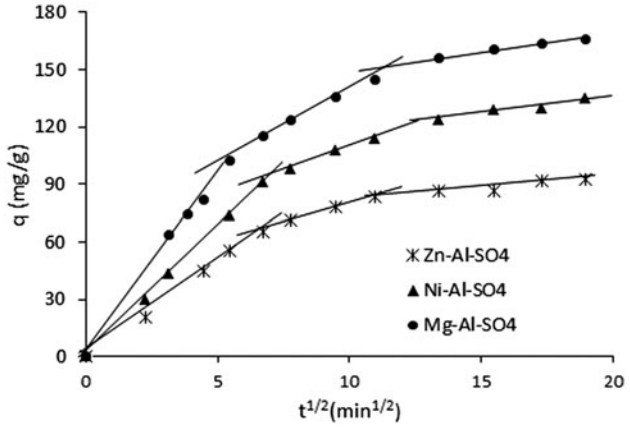

Fig. 7. Intraparticle diffusion model for the adsorption of MO onto LDH samples.

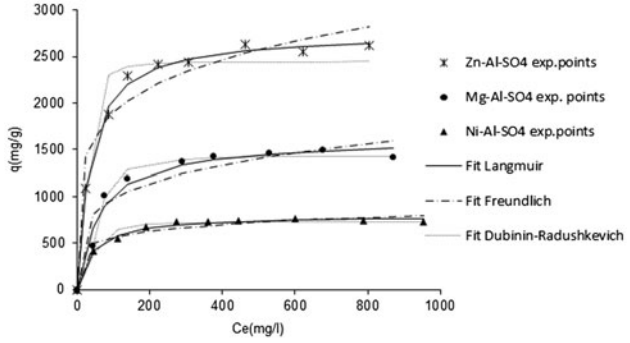

Fig. 8. Isotherms of MO adsorption onto LDH samples (adsorbent dose: 80 mg/l, pH 8, contact time: 8 h, initial MO: 1 g/L, temperature: 25°C, agitation speed: 500 rpm).

solute adsorption (e.g. ionic dyes and metal cations) with weak competition with the solvent molecules. To better understand the adsorption process, the obtained equilibrium adsorption data were analyzed by different isotherm models. An isotherm is characterized by some constants, the values of which express the surface properties and affinity of the LDH. Also that can be used to achieve the adsorption capacity of adsorbents.

In this work, Langmuir, Freundlich, and Dubinin Redushkevich (D–R) isotherm models were evaluated. The parameters obtained from the different models provide important information on the sorption mechanisms and the surface properties and affinities of the sorbent. The Langmuir adsorption model [40] is based on the assumption that the maximum adsorption corresponds to a saturated monolayer of solute molecules on the adsorbent surface. Therefore, the Langmuir isotherm model was chosen for the estimation of the maximum adsorption capacity q_m corresponding to complete monolayer coverage on the sorbent surface. The equation is given as:

$$q_e = \frac{q_m K_L C_e}{1 + K_L C_e} \tag{6}$$

where q_m (mg/g) is the maximum amount of dye adsorbed per unit mass of adsorbent and K_L (L/mg) is the Langmuir constant related to rate of adsorption. C_e is the equilibrium concentration.

The Freundlich isotherm [41] is an empirical equation that assumes that the adsorption surface becomes heterogeneous during the course of the adsorption process. The Freundlich isotherm is expressed by the following equation:

$$q_e = K_F C_e^{1/n} \tag{7}$$

where K_F is a constant for the system, related to the bonding energy, it can be defined as the adsorption or distribution coefficient and represents the quantity of dye adsorbed onto adsorbent for unit equilibrium concentration. $1/n$ indicates the adsorption intensity of the dye onto the sorbent or surface heterogeneity, which becomes more heterogeneous when $1/n$ value gets closer to zero. A value for $1/n$ below 1 indicates a normal Langmuir isotherm, while $1/n$ above 1 indicates a cooperative adsorption

The Dubinin–Radushkevich (D–R) isotherm model does not assume a homogenous surface or constant sorption potential as other models. It can be noted that the (D–R) isotherm is more general that the Langmuir fit [42]. The D–R isotherm has been written by the following equation:

$$q_e = q_m \exp(-B\varepsilon^2) \tag{8}$$

$$\varepsilon^2 = RT \ln\left(1 + \frac{1}{C_e}\right)$$

where B is a constant related to the adsorption energy, q_{max} is the theoretical saturation capacity, ε is the Polanyi potential.

The calculated isotherm parameters for each model and correlation coefficients estimated by nonlinear regressive method are summarized in Table 4. The table indicates that the best fit of experimental data was obtained with the Langmuir model. The values of high r^2 for accused the applicability of the Langmuir model for dye adsorption onto the LDHs. The

Table 4
Model isotherm constants for MO adsorption by LDH samples

	Langmuir models			Freundlich models			Dubinin Radushkevich (D–R)		
Adsorbent	q_m (mg/g)	K_L (L/mg)	R^2	K_F (mg/g) (L/mg)$^{1/n}$	n	R^2	q (mg/g)	B	R^2
Zn–Al-SO_4	2,758.139	0.02832	0.99548	799.4060	5.30391	0.95074	2,447.8760	0.00008	0.85985
Mg–Al-SO_4	1,622.046	0.01617	0.98081	340.2435	4.37985	0.90703	1,433.2941	0.00035	0.96868
Ni–Al-SO_4	800.2345	0.02368	0.98893	275.3328	6.43303	0.94997	727.09822	0.00023	0.8633

maximum Langmuir monolayer adsorption capacity were 2,758, 1,622, and 800 mg/g, respectively, for Zn–Al-SO_4, Mg–Al-SO_4, and Ni–Al-SO_4. This result was in agreement with XRD analysis, demonstrating that Zn–Al-SO_4 presents a high interlayer distance.

3.3. TWW treatment

TWW sample was collected from a polyester and cotton textile mill (ITEX, Casablanca, Morocco) at the factory's discharge point. Table 5 shows the values of various parameters of this effluent. The values show the basic quality of the wastewater sample with a temperature of 30°C and COD value of 614.6 mg/L considered as a point of pollution and does not meet the Moroccan regulatory requirements [43].

To verify the efficiency of LDH samples for TWW treatment, the effects of various parameters on the removal of color and COD by these precursors such as solution pH and adsorbent dose were studied in detail.

3.3.1. Effect of pH on color and COD removal

Fig. 9 shows the changes in the UV–vis spectra of TWW treated by Zn–Al-SO_4 at different solution pH. The result shows that the maximum color reduction obtained at pH 3–5 which is in adequacy with the behavior obtained for MO removal. The influence of pH on COD removal from wastewater by Zn–Al-SO_4 is illustrated in Fig. 10. It was found that the COD removal is more sensitive to pH of wastewater. A maximum COD removal of 90.23% was observed at pH 5 followed by decrease by 50 and 59% at pH 2 and 9.8. The reason for better adsorption capacity observed at lower pH levels might be attributed to the

Table 5
Physicochemical analysis of the TWW

Parameters	Unit	Value	Moroccan standard [43]
pH	_	8.9	5.5–9.0
Temperature	°C	30	30
COD	mg/L	614.6	250
Suspended solid	mg/L	23	150

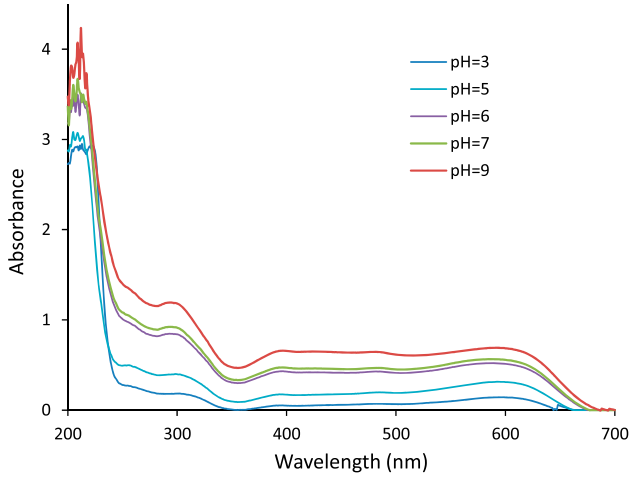

Fig. 9. Evolution of the UV–vis spectra of TWW treated by Zn–Al-SO_4 at different pH solution (V = 20 ml, agitation speed: 500 rpm, initial COD concentration: 614.6 mg/L, time: 8 h, adsorbent dose: 1 g/l).

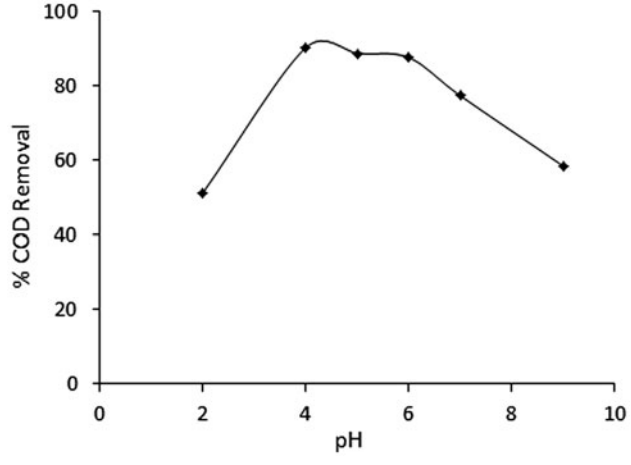

Fig. 10. Effect of pH on COD removal by Zn–Al-SO_4 (V = 20 ml, agitation speed: 500 rpm, initial COD concentration: 614.6 mg/L, time: 8 h, adsorbent dose: 1 g/l).

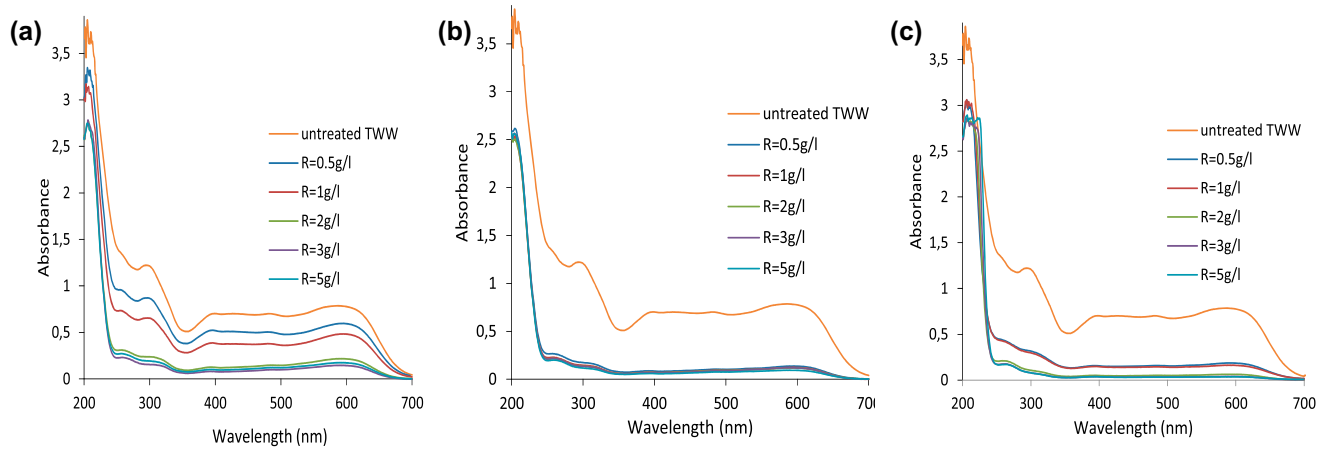

Fig. 11. Variation in UV–vis spectra of TWW at different LDH dosages by: (a) Zn–AlSO$_4$, (b) Mg–Al-SO$_4$, and (c) Ni–Al-SO$_4$ (pH 5, V = 20 mL, and contact time: 8 h).

presence of larger number of H^+ ions. This in turn neutralized the negatively charged adsorbent surface. The lower adsorption values at higher pH may be due to the abundance of OH^- ions. The reduction in percentage of removal at acidic pH was caused by the dissolution of LDH samples at these solution pHs. Similar results were reported for the adsorption of MO.

3.3.2. Effect of adsorbent dose on decolorization

Variation in UV–vis spectra of TWW at different LDH dosages was shown in Fig. 11. The figure shows a considerable decrease in the absorbance with the increase in adsorbent dose. These results attributed by the reduction in chromophore group are responsible for the colorization of TWW. The comparison of the maximum percentage of color removed by various adsorbents shows a rapid decrease in absorbance with the addition of Zn–Al-SO$_4$ and Ni–Al-SO$_4$. It is clear that the color removal was 100% in the case of Ni–Al-SO$_4$ with an amount of 5 g/l. Mg–Al-SO$_4$ shows very large capacity of decolorization at low adsorbent dose. In the case of Zn–Al-SO$_4$, color removal increases successively by the increase in adsorbent dosage.

3.3.3. Effect of adsorbent dosage on COD reduction

The COD is an indication of the overall oxygen load that a wastewater will impose on an effluent stream. COD is equal to the amount of dissolved oxygen that a sample will absorb from a hot acidic solution containing potassium dichromate. The amount of adsorbent, which is usually referred to as the adsorbent dose (grams of adsorbent per 1 L of solution), plays an important role in the adsorption process. The effect of the adsorbent dose on COD removal for the three adsorbents (Zn–Al-SO$_4$, Mg–Al-SO$_4$, and Ni–Al-SO$_4$) was evaluated by varying the dosage from 0.5 to 5 g/L. The results are presented in Fig. 12. The figure indicates that COD removal increases with increasing the amount of adsorbent. The figure also shows that increasing the dose beyond 2 g/L had little effect on the COD reduction, and hence, this value was considered as the optimum. The maximum percentage of COD removed from the TWW was noted as 93.41% for Zn–Al-SO$_4$.

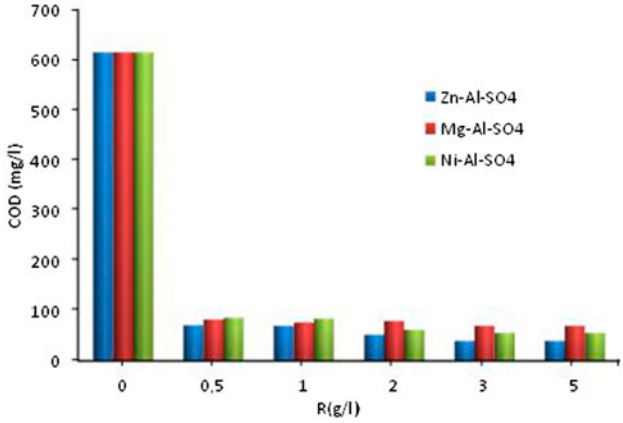

Fig. 12. Effect of adsorbent dosage on the reduction in COD by LDHs (initial COD = 614.6 mg/L, pH 5, V = 20 mL, and time = 8 h).

4. Conclusion

This study evaluated the effect of Zn^{2+}, Mg^{2+}, and Ni^{2+} as divalent cations on the physicochemical properties and dye removal by layered double hydroxides intercalated by SO_4^{2-}. The XRD patterns display high crystallinity of Zn–Al-SO_4 and presented some reductions of crystallinity in Ni–Al-SO_4 and Mg–Al-SO_4. The reduction in sharpness peaks in Mg–Al-SO_4 and Ni–Al-SO_4 should be related to the poor crystallinity or the agglomerates present in the structure which are responsible for the amorphous structure of this sample as confirmed by TEM micrographs. FTIR spectra showed strongly coordinated water and the presence of sulfate in the interlayer. The kinetics of dye removal was better described by intraparticle diffusion model. The equilibrium uptake was increased with increasing the initial concentration of dye in solution. The adsorption isotherm could be well fitted by Langmuir model. It can be concluded that Zn–Al-SO_4 is a promising adsorbent for the treatment of dyes by a reduction in color and COD from cotton TWW.

References

[1] I. Arslan, I. Akmehmet Balcioğlu, Degradation of commercial reactive dyestuffs by heterogenous and homogenous advanced oxidation processes: A comparative study, Dyes Pigm. 43 (1999) 95–108.

[2] M. Kornaros, G. Lyberatos, Biological treatment of wastewaters from a dye manufacturing company using a trickling filter, J. Hazard. Mater. 136 (2006) 95–102.

[3] S.S. Moghaddam, M.R.A. Moghaddam, M. Arami, Coagulation/flocculation process for dye removal using sludge from water treatment plant: Optimization through response surface methodology, J. Hazard. Mater. 175 (2010) 651–657.

[4] K. Dutta, S. Mukhopadhyay, S. Bhattacharjee, B. Chaudhuri, Chemical oxidation of methylene blue using a Fenton-like reaction, J. Hazard. Mater. 84 (2001) 57–71.

[5] G. Capar, U. Yetis, L. Yilmaz, Membrane based strategies for the pre-treatment of acid dye bath wastewaters, J. Hazard. Mater. 135 (2006) 423–430.

[6] S. Karcher, A. Kornmüller, M. Jekel, Anion exchange resins for removal of reactive dyes from textile wastewaters, Water Res. 36 (2002) 4717–4724.

[7] A. Abaamrane, S. Qourzal, N. Barka, S. Billah, A. Assabbane, Y. Ait-Ichou, Optimal decolorization efficiency of indigo carmine by TiO_2/UV photocatalytic process coupled with response surface methodology, Orient. J. Chem. 28 (2012) 1091–1098.

[8] R. Elmoubarki, F.Z. Mahjoubi, H. Tounsadi, J. Moustadraf, M. Abdennouri, A. Zouhri, A. El Albani, N. Barka, Adsorption of textile dyes on raw and decanted Moroccan clays: Kinetics, equilibrium and thermodynamics, Water Resour. Ind. 9 (2015) 16–29.

[9] G. Crini, Non-conventional low-cost adsorbents for dye removal: A review, Bioresour. Technol. 97 (2006) 1061–1085.

[10] N. Barka, K. Ouzaouit, M. Abdennouri, M. Makhfouk, Dried prickly pear cactus (Opuntia ficus indica) cladodes as a low-cost and eco-friendly biosorbent for dyes removal from aqueous solutions, J. Taiwan Inst. Chem. Eng. 44 (2013) 52–60.

[11] N. Barka, A. Assabbane, Y. Aît Ichou, A. Nounah, Decantamination of textile wastewater by powdered activated carbon, J. Appl. Sci. 63 (2006) 692–695.

[12] N. Barka, A. Assabbane, A. Nounah, L. Laanab, Y. Ichou, Removal of textile dyes from aqueous solutions by natural phosphate as a new adsorbent, Desalination 235 (2009) 264–275.

[13] L. Ai, Y. Zhou, J. Jiang, Removal of methylene blue from aqueous solution by montmorillonite/$CoFe_2O_4$ composite with magnetic separation performance, Desalination 266 (2011) 72–77.

[14] M.M. Nassar, M.S. El-Geundi, Comparative cost of colour removal from textile effluents using natural adsorbents, J. Chem. Technol. Biotechnol. 50 (1991) 257–264.

[15] R.S. Juang, F.C. Wu, R.L. Tseng, The ability of activated clay for the adsorption of dyes from aqueous solutions, Environ. Technol. 18 (1997) 525–531.

[16] F. Cavani, F. Trifirò, A. Vaccari, Hydrotalcite-type anionic clays: Preparation, properties and applications, Catal. Today 11 (1991) 173–301.

[17] L. Raki, D.G. Rancourt, C. Detellier, Preparation, characterization, and Moessbauer spectroscopy of organic anion intercalated pyroaurite-like layered double hydroxides, Chem. Mater. 7 (1995) 221–224.

[18] N.T.P. Whilton, P.J. Vickers, S. Mann, Bioinorganic clays: Synthesis and characterization of amino- and polyamino acid intercalated layered double hydroxides, J. Mater. Chem. 7 (1997) 1623–1629.

[19] E. Lopez-Salinas, Y. Ono, Intercalation chemistry of a Mg–Al layered double hydroxide ion-exchanged with complex MCl_4^{2-} (M = Ni, Co) ions from organic media, Microporous Mater. 1 (1993) 33–42.

[20] S. Carlino, The intercalation of carboxylic acids into layered double hydroxides: A critical evaluation and review of the different methods, Solid State Ionics 98 (1997) 73–84.

[21] X. Hou, D.L. Bish, S.-L. Wang, C.T. Johnston, R.J. Kirkpatrick, Hydration, expansion, structure, and dynamics of layered double hydroxides, Am. Mineral. 88 (2003) 167–179.

[22] T. Witzke, G. Raade, Zincowoodwardite [$Zn_{1-x}Al_x(SO_4)_x/2(OH)_2{\cdot}(H_2O)_n$], a new mineral of the hydrotalcite group, N.J. Miner. M. 10 (2000) 455–465.

[23] J.S. Noh, J.A. Schwarz, Estimation of the point of zero charge of simple oxides by mass titration, J. Colloid Interface Sci. 130 (1989) 157–164.

[24] A.E. Greenberg, L.S. Clesceri, A.D. Eaton, Standard methods: For the examination of water and wastewater, eighteenth ed., American Public Health Association (APHA), Washington, DC, 1992.

[25] R.D. Shannon, Revised effective ionic radii and systematic studies of interatomic distances in halides and chalcogenides, Acta Crystallogr. Sect. A 32 (1976) 751–767.

[26] J. Sanchez Valente, F. Figueras, M. Gravelle, P. Kumbhar, J. Lopez, J.-P. Bessey, Basic properties of the mixed oxides obtained by thermal decomposition of hydrotalcites containing different metallic compositions, J. Catal. 189 (2000) 370–381.
[27] R.L. Frost, M.L. Weier, J.T. Kloprogge, Raman spectroscopy of some natural hydrotalcites with sulphate and carbonate in the interlayer, J. Raman Spectrosc. 34 (2003) 760–768.
[28] R.L. Frost, A.W. Musumeci, J.T. Kloprogge, M.O. Adebajo, W.N. Martens, Raman spectroscopy of hydrotalcites with phosphate in the interlayer: Implications for the removal of phosphate from water, J. Raman Spectrosc. 37 (2006) 733–741.
[29] S. Narayanan, K. Krishna, Hydrotalcite-supported palladium catalysts, Appl. Catal. A: Gen. 174 (1998) 221–229.
[30] M.J. Hernandez-Moreno, M.A. Ulibarri, J.L. Rendon, C.J. Serna, IR characteristics of hydrotalcite-like compounds, Phys. Chem. Mater. 12 (1985) 34–38.
[31] D.L. Bish, A. Livingstone, The crystal chemistry and paragenesis of honessite and hydrohonessite: The sulphate analogues of reevesite, Mineral. Mag. 44 (1981) 339–343.
[32] L. Cocheci, P. Barvinschi, R. Pode, E. Popovici, E.M. Seftel, Structural characterization of Some Mg/Zn–Al type hydrotalcites prepared for chromate sorption from wastewater, Chem. Bull. 55 (2010) 40–45.
[33] R.V. Prikhod'k, M.V. Sychev, I.M. Astrelin, K. Erdmann, A. Mangel', R.A. van Santen, Synthesis and structural transformations of hydrotalcite-like materials Mg–Al and Zn–Al. Russ. J. Appl. Chem. 74 (2001) 1621–1626.
[34] F. Kooli, C. Depege, A. Ennaqadi, A. De Roy, J.P. Besse, Rehydration of Zn–Al layered double hydroxides, Clays Clay Miner. 45 (1997) 92–98.
[35] S. Lagergren, About the theorie of so-called adsorption of soluble substance Seven Vetenskapsakad, Handband 24 (1898) 1–39.
[36] Y.S. Ho, G. McKay, Pseudo-second order model for sorption processes, Process Biochem. 34 (1999) 451–465.
[37] Y. Li, B. Gao, T. Wu, B. Wang, X. Li, Adsorption properties of aluminum magnesium mixed hydroxide for the model anionic dye Reactive Brilliant Red K-2BP, J. Hazard. Mater. 164 (2009) 1098–1104.
[38] W. Weber, J. Morris, Kinetics of adsorption on carbon from solution, J. Sanit. Eng. Div. Am. Soc. Civ. Eng. 89 (1963) 31–59.
[39] C.H. Giles, T.H. MacEwan, S.N. Nakhwa, D. Smith, Studies in adsorption. Part XI. A system of classification of solution adsorption isotherms and its use in diagnosis of adsorption mechanisms and in measurement specific surface of solids, J. Chem. Soc. (Resumed) 111 (1960) 3973–3993.
[40] I. Langmuir, The constitution and fundamental properties of solids and liquids. Part I. Solids, J. Am. Chem. Soc. 38 (1916) 2221–2295.
[41] H. Freundlich, W. Heller, The adsorption of cis- and trans-azobenzene, J. Am. Chem. Soc. 61 (1939) 2228–2230.
[42] M.M. Dubinin, L.V. Radushkevich, The equation of the characteristic curve of the activated charcoal, Proc. Acad. Sci. USSR Phys. Chem. Sec. 55 (1947) 331–337.
[43] Ministry of the Environment of Morocco, Moroccan Standards, Morocco's Official Bulletin, No. 5062, Rabat, 2002.